Kinetic-Dependent Crystal Growth of Size-Tunable CdS Nanoparticles

Chung-Sung Yang,† David D. Awschalom,‡ and Galen D. Stucky*,†

Department of Chemistry and Biochemistry, Materials Research Laboratory, Department of Physics, University of California, Santa Barbara, California 93106

Received June 29, 2000. Revised Manuscript Received September 25, 2000

The general study of crystal growth of spherical-like nanoparticles involves monitoring the kinetics during the progress of the reaction. In the case of cadmium sulfide (CdS), cadmium acetate and sodium sulfide are employed as starting reagents that are dissolved in different solvents (ethylene glycol, glyme, diglyme, and trioctylphosphine) to study the solvent effect on monomers, nucleation rates, and the quality of the seeds. Trialkylphosphine oxide (alkyl = ethyl or octyl) is chosen as a surfactant to passivate the surface of CdS nanoparticles. We propose a kinetic approach model to illustrate the unreported time-evolved crystal growth mechanism observed in this case. An experimental value for the diameter of critical volume (V_c), a nanosized volume with a relative minimum surface-volume tension and considered a temporal stable stage ($r = 5.7$ nm in this case), is derived from transmission electron microscopy images. The size of the nanoparticles made by this synthesis route is tunable by variation of the reaction time and control of the reaction temperature; in addition, the resulting sizes are suitable for spectroscopic testing of electron quantum confinement. The X-ray powder diffraction data are consistent with a pure hexagonal CdS lattice and show no evidence for a mixed phase involving cubic symmetry.

Introduction

Colloidal semiconductor nanoclusters have been intensively investigated for the past decade[1−4] because of their unusual magnetic[5] and optical properties.[6] There are many well-developed synthetic routess that attempt to provide control over the size distribution and, eventually, a monodisperse size[7−14] that is critically important for defining size-dependent optoelectronic properties due to the quantum confinement of electrons.[6,15,16] However, the most demanding requirement is that these nanoparticles can be custom-designed for their optoelectronic application purpose[17] and, potentially, mass-produced. Synthesis methods employing polymers and glasses produce size-polydisperse products.[18,19] Zeolites limit nanoparticle diameters to pore dimensions[16,20,21] and lithographic technology cannot reach the necessary resolution[16,22] to synthesize size-quantized II−VI materials, such as CdS or CdSe. Ion-sputtering technology produces crystalline GaSb quantum dots 35 nm in diameter that are arranged in a regular hexagonal lattice but has not been used for CdS.[23] Reverse/inverse micelle systems, generally used in the preparation of metal nanoparticles, with surfactants and copolymers give a well-controlled size distribution with the diameter smaller than that of the micelles.[24,25] Sol−gel methods with the aging of a highly concentrated solution of Cd^{2+} ion in combination with chelating agents at room temperature can produce a uniform-disperse product with a mean diameter from 43.9 to 249 nm.[26] Single-molecule precursors synthetic approaches offer high-

* To whom correspondence should be addressed.
† Department of Chemistry and Biochemistry.
‡ Department of Physics.

(1) Steigerwald, M. L.; Brus, L. E. *Annu. Rev. Mater. Sci.* **1989**, *19*, 471−495.
(2) Schmid, G. *Chem. Rev.* **1992**, *92*, 1709−1727.
(3) Alivisatos, A. P. *J. Phys. Chem.* **1996**, *100*, 13226−13239.
(4) Alivisatos, A. P.; Barbara, P. F.; Castleman, A. W.; Chang, J.; Dixon, D. A.; Klein, M. L.; McLendon, G. L.; Miller, J. S.; Ratner, M. A.; Rossky, P. J.; Stupp, S., I.; Thompson, M. E. *Adv. Mater.* **1998**, *10*, 1297−1336.
(5) Shi, J.; Babcock, G. K.; Awschalom, D. D. *Science* **1996**, *271*, 937−941.
(6) Alivisatos, A. P. *Science* **1996**, *271*, 933−937.
(7) Dameron, C. T.; Reese, R. N.; Mehra, R. K.; Kortan, A. R.; Carroll, P. J.; Steigerwald, M. L.; Brus, L. E.; Winge, D. R. *Nature* **1989**, *338*, 596−597.
(8) Korgel, B. A.; Monbouquette, H. G. *J. Phys. Chem.* **1996**, *100*, 346−351.
(9) Lazell, M.; O'Brien, P. *Chem. Commun.* **1999**, 2041−2042.
(10) Murray, C. B.; Norris, D. J.; Bawendi, M. G. *J. Am. Chem. Soc.* **1993**, *115*, 8706−8715.
(11) Peng, X.; Manna, L.; Yang, W.; Wickham, J.; Scher, E.; Kadavanich, A.; Alivisatos, A. P. *Nature* **2000**, *404*, 59−61.
(12) Torimoto, T.; Kontani, H.; Sakata, T.; Mori, H.; Yoneyama, H. *Chem. Lett.* **1999**, 379−380.
(13) Trindade, T.; O'Brien, P. *J. Mater. Chem.* **1996**, *6*, 343−347.
(14) Colvin, V. L.; Schlamp, M. C.; Alivisatos, A. P. *Nature* **1994**, *370*, 354−356.
(15) Brus, L. E. *J. Phys. Chem.* **1986**, *90*, 2555−2560.
(16) Stucky, G. D.; MacDougall, J. E. *Science* **1990**, *247*, 669−678.
(17) Bruchez, M. J.; Moronne, M.; Gin, P.; Weiss, S.; Alivisatos, A. P. *Science* **1998**, *281*, 2013−2016.
(18) Nirmal, M.; Murray, C. B.; Bawendi, M. G. *Phys. Rev. B* **1994**, *50*, 2293−2300.
(19) Huang, J.; Yang, Y.; Yang, B.; Liu, S.; Shen, J. *Polym. Bull.* **1996**, *36*, 337−340.
(20) Yang, P.; Zhao, D.; Margolese, D. I.; Chmelka, B. F.; Stucky, G. D. *Nature* **1998**, *396*, 152−154.
(21) Hirai, T.; Okubo, H.; Kamasawa, I. *J. Phys. Chem. B* **1999**, *103*, 4228−4230.
(22) Weller, H. *Angew. Chem., Int. Ed. Engl.* **1993**, *32*, 41−53.
(23) Facsko, S.; Dekorsy, T.; Koerdt, C.; Trappe, C.; Kurz, H.; Vogt, A.; Hartnagel, H. L. *Science* **1999**, *285*, 1551−1553.
(24) Pileni, M. P. *Langmuir* **1997**, *13*, 3266−3276.
(25) Lin, X. M.; Sorensen, C. M.; Klabunde, K. J.; Hajipanayis, G. C. *L. Mater. Res.* **1999**, *14*, 1542−1547.

10.1021/cm0005384 CCC: $20.00
Published on Web 01/06/2001

quality CdS or CdSe nanoparticles obtained by re-isolation and re-dispersion of the product to reach an average size and size distribution of 50 ± 8 Å.[27] A thermolysis method using trioctylphosphine sulfide (TOPS) can produce similar quality CdS nanoparticles by refluxing air-sensitive starting reagents with TOPO but the yield and size distribution data are not available.[13] Solution syntheses that employ polymer-matrix-encapsulation methods to grow CdS nanoparticles inside a polymer network can make very small nanoclusters with diameters from 15 to 55 Å but thermal annealing is needed to improve the crystallinity of the product.[28] The most promising of current technologies to offer monodisperse nanoparticles is the use of coordinating solvents and stabilizing agents to control particle nucleation, crystal growth, and final particle size.[11,29−36] In this report, we present a reliable solution synthesis route using non-air-sensitive starting reagents to produce size-tunable, high-quality monodisperse nanoparticles with a standard deviation as small as 5.9%. The tightest size distribution reported to date is ≈5.0% using highly air-sensitive starting reagents.[10] The subsequent processing steps to narrow down the size distribution and/or to improve the quality of nanoparticles are not necessary in our case.

Experimental Section

Chemicals. Cadmium acetate and sodium sulfide were purchased from Aldrich. Reagent-grade ethylene glycol (EG) (99.5% Aldrich), ethylene glycol dimethyl ether (glyme) (99.5% Aldrich), 2-methoxyethyl ether (diglyme) (99+%), triethylphosphine oxide (TEPO) (99.9% Aldrich), and trioctylphosphine oxide (TOPO) (99% Aldrich) were used without any further purification. HPLC-grade hexane and methanol and reagent-grade 1-butanol were obtained from Aldrich and used as supplied.

Synthesis and Characterization. The CdS nanoparticles were synthesized via the reaction of cadmium acetate and sodium sulfide in a Schlenk line N_2 atmosphere. The starting reagents (1.0 mmol for each precusor) were dissolved completely in selected solvents (20 mL) and kept as a stock solution. A 1.5-mL stock solution was injected into a hot surfactant solvent (5.0 g) (TEPO, 215 °C or TOPO, 340 °C) as the initial source of monomers. The color of solution changed from orange to deep orange during the reaction. A second injection (0.2 mL) was added at the 120th min. At the growth temperature (200−230 °C), aliquots (0.2−0.3 mL for each withdrawn) were taken to calibrate the quality of the nanoparticles by ultraviolet−visible and photoluminescence spectroscopy and the crystal size by transmission electron microscopy and X-ray powder diffraction. Each product was washed with 10 mL of methanol twice and then 15 mL of 1-butanol to remove surfactant residue completely. The final orange precipitate can be dried as a powder or re-suspended in methanol or 1-butanol.

Table 1. Synthesis Condition and Results of CdS Nanoparticles[a]

sample	solvent	surfactant	time	size of QD
1	80% glyme + 20% EG	TEPO	50	3.0−15.0 nm
2	80% glyme + 20% EG	TOPO	50	4.0−15.0 nm
3	glyme	TOPO	50	x
4	80% diglyme + 20% EG	TEPO	50	4.0−10.0 nm
5	80% diglyme + 20% EG	TOPO	50	5.0−7.0 nm
6	diglym	TOPO	50	x
7	TOP	TOPO	50	x
8	EG	TOPO	50	x

[a] TEPO = triethylphosphine oxide; TOPO = trioctylphosphine oxide; x = product shows no convincing evidence for nanoparticles under TEM.

X-ray powder diffraction data were obtained on a Scintag 4000. Data were measured at room temperature using Cu $K\alpha_1$ radiation. Transmission electron microscopy (TEM) images were collected on a JEOL 2000FX and 2010 HR and both are with a 200-kV accelerating voltage. Samples were prepared by evaporation of the colloidal solution onto a 300-mesh Cu grid. Optical absorption spectra of methanol colloids in a quartz cell were obtained with a Shimadzu UV 1601 spectrophotometer. Photoluminescence spectra were obtained from a SPEX FluoroMax spectrophotometer with an excitation wavelength at 360 nm. All spectra were collected at room temperature.

Results and Discussion

The synthesis conditions and results obtained for CdS nanoparticles are given in Table 1. The size distribution and quality of nanoparticles vary with coordinating solvent and surfactant. The reaction temperature also contributes to the determination of nanocrystal quality.[22] The synthesis route of sample 5 was selected to evaluate the reaction progress for CdS due to its reliable yield (>60%) and tight size distribution. After injection of stock monomers into hot TOPO (350−330 °C), nucleation occurred immediately, followed by competition between decomposition and nucleation of seeds. The competition mechanism observed in CdS is different from that of CdSe because of the obvious difference in ionic solubility product between CdS ($K_{sp} = 1.4 \times 10^{-19}$) and CdSe ($K_{sp} = 1.4 \times 10^{-34}$). A detailed competition mechanism is illustrated in the following paragraph. The temperature was set between 230 and 200 °C to favor the equilibrium between seeds and monomers. The precise kinetics of nucleation and decomposition between seeds and monomers are difficult to study. However, the equilibria between nucleation and decomposition are known to be highly dependent on temperature and concentration.[11,22,37]

Figure 1 shows four TEM micrographs for different progress times (22, 50, 100, and 150 min) during the synthesis. After 22 min from the initial injection, equilibrium has been reached. The seeds surviving from the competition grow quickly to V_c size but some smaller seeds decompose back to monomers, as shown in Figure

(26) Sugimoto, T.; Chen, S.; Muramatsu, A. *Colloids Surf. A* **1997**, *135*, 207−226.
(27) Trindade, T.; O'Brien, P.; Zhang, X.-m. *Chem. Mater.* **1997**, *9*, 523−530.
(28) Olshavsky, M. A.; Allcock, H. R. *Chem. Mater.* **1997**, *9*, 1367−1376.
(29) Spanhel, L.; Haase, M.; Weller, H.; Henglein, A. *J. Am. Chem. Soc.* **1987**, *109*, 5649−5655.
(30) Steigerwald, M. L.; Alivisatos, A. P.; Gibson, J. M.; Harris, T. D.; Kortan, R.; Muller, A. J.; Thayer, A. M.; Dancan, T. M.; Douglass, D. C.; Brus, L. E. *J. Am. Chem. Soc.* **1988**, *110*, 3046−3050.
(31) Bawendi, M. G.; Kortan, A. R.; Steigerwald, M. L.; Brus, L. E. *J. Chem. Phys.* **1989**, *91*, 7282.
(32) Kortan, A. R.; Hull, R.; Opila, R. L.; Bawendi, M. G.; Steigerwald, M. L.; Carroll, P. J.; Brus, L. E. *J. Am. Chem. Soc.* **1990**, *112*, 1327−1332.
(33) Herron, N.; Wang, Y.; Eckert, H. *J. Am. Chem. Soc.* **1990**, *112*, 1322−1326.
(34) Colvin, V. L.; Goldstein, A. N.; Alivisatos, A. P. *J. Am. Chem. Soc.* **1992**, *114*, 5221−5525.
(35) Roberti, T. W.; Cherepy, N. J.; Zhang, J. Z. *J. Phys. Chem.* **1998**, *V108*, 2143-2151.
(36) Yang, C.-S.; Bley, R. A.; Kauzlarich, S. M.; Lee, H. W. H.; Delgado, G. R. *J. Am. Chem. Soc.* **1999**, *121*, 5191−5195.
(37) Peng, X.; Wickham, J.; Alivisatos, A. P. *J. Am. Chem. Soc.* **1998**, *120*, 5343−5344.

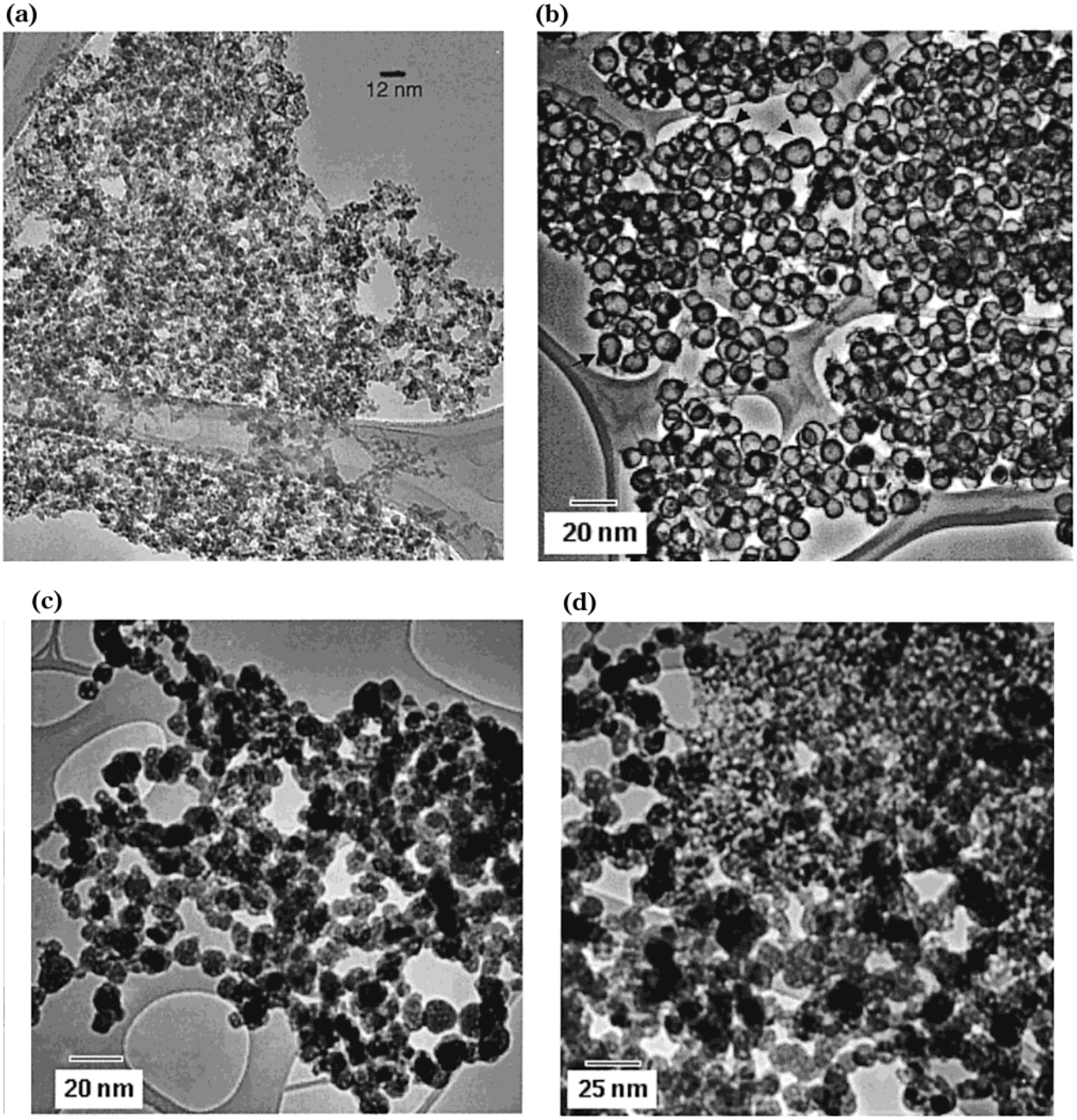

Figure 1. TEM images for samples with different progress times: (a) 22 min, a large number of small size (3−4 nm) nanocrystals are shown. (b) 50 min, in this regime, the size of nanoparticles is convergent with a standard derivation (σ) of 5.9%. The average diameter of V_c and σ is taken over more than 250 roughly spherical nanoparticles but the irregular ones were intentionally ignored, ≈4% of the total number of nanoparticles, as marked with short arrows in this image. (c) 100 min, size lost convergence. Some V_c particles crossed over E_b^* and reached the bulk regime. Aggregation of nanoparticles is observed at this step. (d) 150 min, new small size nanoparticles are shown after the second injection (at the 120th min). Aggregation is still observed in this micrograph.

1a. The 50-min TEM image, Figure 1b, shows that the average size of nanoparticles increases slowly upon reaching V_c. Size distribution focusing phenomena are observed at this step. An experimental V_c value, 5.7 nm with a standard derivation of 5.9%, is calculated by calibrating the nanoparticles sizes from four TEM images of a 50-min sample; the average is taken over more than 250 roughly spherical nanoparticles but intentionally ignored the irregular ones in the images, ≈4% of the total number of nanoparticles, as marked with short arrows in Figure 1b. The size value calculated from the X-ray diffraction pattern of the same sample is about 8−15% larger than that obtained from TEM images and is considered consistent. The V_c value derived from TEM micrographs is potentially smaller than the real one because only the average size and the variance are considered but not the possibility of asymmetry of distribution and nonspherical particles.[37] A more accurate experimental method of sizing will be required to determine the V_c value. Figure 1c (100 min) shows that some V_c nanoparticles crossed over the activation energy of bulk (E_b^*) and reached the bulk regime, while a large number of nanoparticles remain the V_c size. Aggregation occurs obviously at this step in

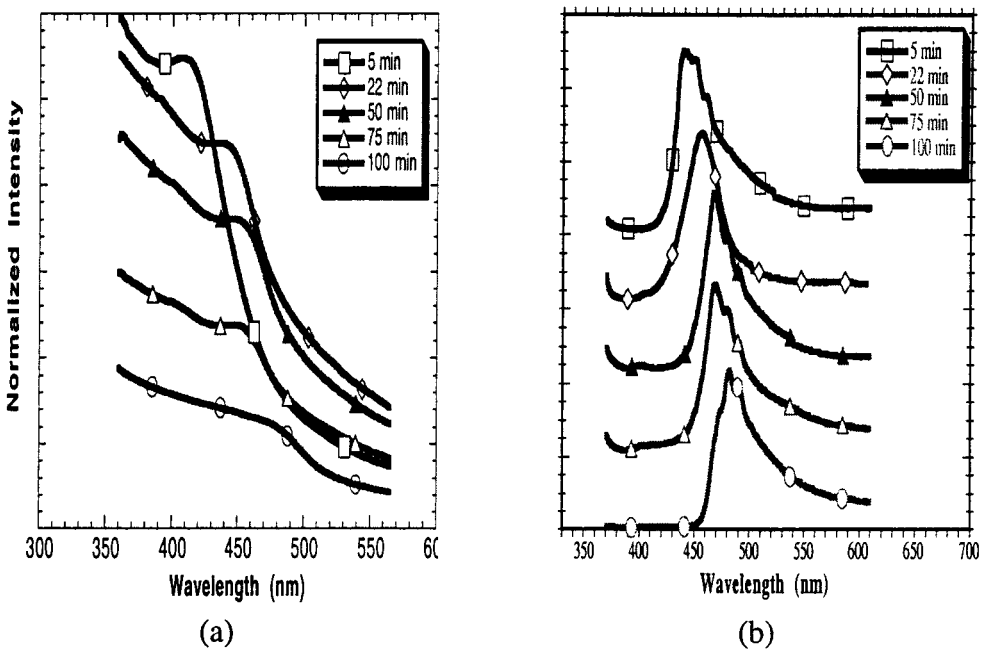

Figure 2. Room-temperature absorption (left) and photoluminescence spectra (right) for samples with different progress times. The sharp UV spectra and narrow half width of PL spectra, smaller than 50 nm, indicate tight size distribution and good crystal quality.

both bulk and V_c size nanocrystals. New monomers (0.2 mL) were injected at the 120th min to study the concentration factor. The size distribution is expected to refocus and the average size may be shifted back to a smaller value because new nanocrystalline seeds will be produced at the new equilibrium. Figure 1d (150 min) shows a large number of aggregated bulk size particles (>20 nm) and V_c nanoparticles mixed with some small size nanocrystals (3−4 nm); the latter sizes were not seen in the 100-min TEM image. The existence of these small nanoparticles in the 150-min TEM image suggests that a new equilibrium has been reached and new crystalline seeds were formed.

Figure 2 shows the UV−visible absorption spectra and photoluminescence spectra for five different progress times for sample 5. A red shift is observed in both spectra as the reaction time increases. The absorption peaks of these products are relatively sharp, which indicates a tight size distribution and good crystal quality.[10,30] The half-width of the PL peak is smaller than 50 nm and is similar to that of the UV−vis peak. The long tail peak associated with deep trap states due to surface or core defects is not evident in these samples.[8,38,39] The quantum yield, using Rhodamine as a standard (=1.0) and measured with the same optical density, is about 0.55−0.65 at room temperature. These experimental results suggest that the CdS nanoparticles have relatively good quantum efficiency (small difference in half-width between PL and UV−vis peak) and quantum yield so that these nanoparticles are of the quality necessary for the study of quantum confinement theory.

The time-evolved size distribution and standard derivation (%) of sample 6 are shown in Figure 3. The

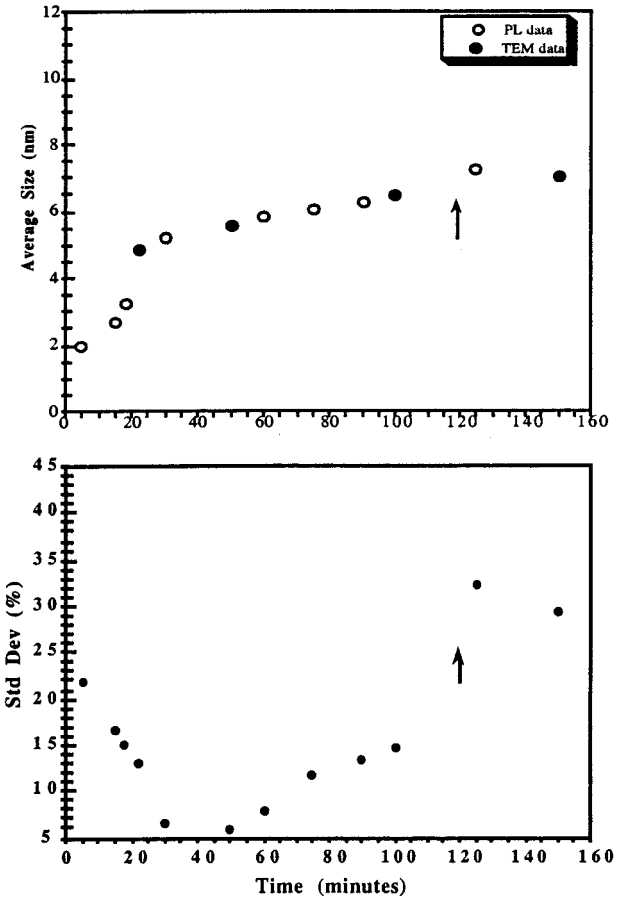

Figure 3. Average size distribution and standard derivation. The data extracted from PL spectra are marked with an open circle and those extracted from TEM images are marked with a filled circle in the average size figure. The arrow indicates the time of the second injection.

size data extracted from PL spectra, by assuming each size has the same emission function and the same emission efficiency for different sizes, are marked with

(38) Bawendi, M. G.; Wilson, W. L.; Rothberg, L.; Carroll, P. J.; Jedju, T. M.; Steigerwald, M. L.; Brus, L. E. *Phys. Rev. Lett.* **1990**, *65*, 1623−1626.

(39) Bawendi, M. G.; Carroll, P. J.; Wilson, W. L.; Brus, L. E. *J. Chem. Phys.* **1992**, *96*, 946−954.

Scheme 1. CdS Nanocrystal Growth

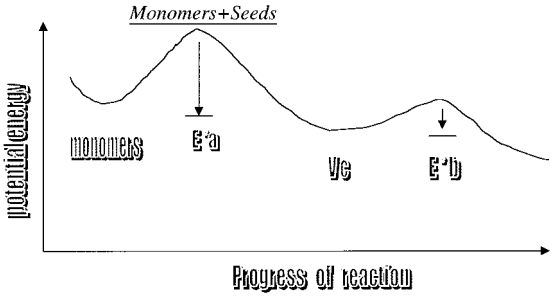

open circles. Data measured directly from TEM images using the average value of size of well-defined spherical nanoparticles are marked with filled circles. In the nucleation step, the average size increases quickly and the standard derivation decreases simultaneously. As the reaction approaches the size convergence regime (30−75 min), the growth speed of nanoparticles slows down to give an average size of 5.2−5.8 nm and a relatively small standard derivation (5.9−7.9%). TEM images taken at different reaction times revealed that the number of particles are approximately similar in the convergence regime but decrease in the divergence regime. This result is consistent with our model, see below, and with the literature.[37] After new monomers are injected at the 120th min, all particles grow again and similar growth kinetics are observed in 125 and 150-min samples. The average size of the 150th-min sample shrinks 6.8% relative to the 125-min sample. This implies that refocusing of the average size has occurred. If the bulk size particles are removed from calculation, the size deviation of new nanoparticles for the 150-min sample can be as small as 11.2%.

We propose a time-evolved, kinetic-dependent model, based on the phenomena observed in our experimental results, to monitor the mechanism of CdS nanocrystal growth from the initial nucleation to bulk size regime, as shown in Scheme 1. In the initial step, crystalline seeds are formed suddenly after the injection of monomers. The sizes of the seeds are somewhat different and reaction is followed by competition between decomposition and nucleation. Larger seeds surviving from competition cross over the activation energy barrier (E_a^*) and grow toward the size of critical volume (V_c). On the other hand, smaller seeds are still in the competition or even decompose back to monomers. The size distribution diverges due to the different growth speeds.[1,22,37] The competition mechanism is shown in the following equations:

$$m\mathrm{Cd}^{2+} + n\mathrm{S}^{2-} \rightarrow (\mathrm{CdS})_x + (\mathrm{CdS})_y + (\mathrm{CdS})_z + (m-x-y-z)\mathrm{Cd}^{2+} + (m-x-y-z)\mathrm{S}^{2-} \quad (1)$$

$$(\mathrm{CdS})_x \rightarrow (\mathrm{CdS})_{x-1} + \mathrm{Cd}^{2+} + \mathrm{S}^{2-} \quad (2a)$$

$$\mathrm{Cd}^{2+} + \mathrm{S}^{2-} + (\mathrm{CdS})_y \rightarrow (\mathrm{CdS})_{y+1} \text{ or } (\mathrm{CdS})_y \rightarrow (\mathrm{CdS})_{y-1} + \mathrm{Cd}^{2+} + \mathrm{S}^{2-} \quad (2b)$$

$$\mathrm{Cd}^{2+} + \mathrm{S}^{2-} + (\mathrm{CdS})_z \rightarrow (\mathrm{CdS})_{z+1} \quad (2c)$$

($m, n \gg x, y, z$ and $z > y > x$)

Then, the system reaches equilibrium through the depletion of smaller seeds, $(\mathrm{CdS})_x$. The concentration of monomers and the number of seeds remain constant before equilibrium is lost. All seeds grow at this step. However, bigger seeds, such as $(\mathrm{CdS})_z$, grow more quickly than others to reach the V_c size. Upon reaching or slightly passing over V_c, a relative lower potential state, the V_c size nanoparticles slow growth speed. But newly surviving competition seeds, $(\mathrm{CdS})_y$, just passing over the energy barrier E_a^*, grow quickly toward V_c. The size distribution of nanoparticles converges gradually at this step. It is possible to obtain monodisperse nanoparticles ($\sigma < 7.0\%$) by stopping the progress of the reaction in the time period of the size convergence regime. If the reaction is allowed to continue after the V_c time, early V_c nanoparticles, formed by $(\mathrm{CdS})_z$, will begin crossing over E_b^* and grow slowly to bulk size, the final stable state. Particle sizes smaller than V_c nanocrystals, such as $(\mathrm{CdS})_{y-1}$, decompose gradually and provide monomers for nanoparticles crossing over E_b^* to grow. Meanwhile, the new V_c nanoparticles, formed by $(\mathrm{CdS})_y$, maintain or change their sizes slightly. After depleting all available $(\mathrm{CdS})_{y-1}$ seeds, there is no other source of monomers to maintain the equilibrium concentration of monomers. The equilibrium of the system is lost and convergence of the size distribution is no longer possible.

Summary

A time evolution kinetic-dependent crystal growth model has been proposed to monitor the nanocrystal growth mechanism of CdS in a solution synthesis. Photoluminescence spectra, UV−visible spectra, X-ray powder diffraction, and TEM images were employed to calibrate the V_c value and the average size of products with different progress times. The sharp UV−visible and narrow photoluminescence peaks indicate a tight size distribution and good crystal quality. The average size distribution and size standard derivation were derived from PL spectra and TEM images. In the size convergence regime, an average size distribution from 5.2 to 5.8 nm was observed. The V_c value (5.7 nm with $\sigma = 5.9\%$) is calculated from the size data shown in four TEM images of a 50-min progress time sample by ignoring the possibility of asymmetry of distribution and nonspherical particles. As new monomers were added, a refocus of the V_c size and re-convergence of size distribution phenomena occur as the reaction reaches a new equilibrium.

Acknowledgment. The authors are grateful to the National Science Foundation (Grant DMR 96-34396 and DMR 98-71849) and Office of Naval Research ONR N00014-99-1-0728 for financial support. C.-S.Y. thanks Celia Wrathall for helping to revise the manuscript. Work at the Material Research Laboratory, University of California Santa Barbara, make use of the MRL Center Facilities supported by the National Science Foundation under Award DMR 96-32716.

Supporting Information Available: Typical X-ray powder diffraction pattern for aliquots taken from sample 6 with 22-, 50-, and 100-min progress time (PDF). This material is available free of charge via the Internet at http://pubs.acs.org.

CM0005384